JACS
JOURNAL OF THE AMERICAN CHEMICAL SOCIETY
pubs.acs.org/JACS
Communication

Recombinant Expression and Chemical Amidation of Isotopically Labeled Native Melittin

Martin D. Gelenter and Ad Bax*

Cite This: J. Am. Chem. Soc. 2023, 145, 3850−3854
Read Online
ACCESS | Metrics & More | Article Recommendations | Supporting Information

ABSTRACT: Post-translational modifications are ubiquitous in the eukaryotic proteome. However, these modifications are rarely incorporated in NMR studies of eukaryotic proteins, which are typically produced through recombinant expression in *E. coli*. Melittin is the primary peptide in honey bee venom. Its native C-terminal amide significantly affects its equilibrium structure and dynamics in solution and is thus a prerequisite for studying its native structure and function. Here, we present a method for producing triply isotopically labeled (^{2}H, ^{13}C, and ^{15}N) native melittin through recombinant expression followed by chemical amidation. We then show that structural models produced with AlphaFold-Multimer are in even better agreement with experimental residual dipolar couplings than the 2.0 Å resolution X-ray crystal structure for residues G3−K23.

Melittin, the primary active component in honey bee venom, is a membrane-lytic peptide that is post-translationally amidated at the C-terminus. Like melittin, many antimicrobial peptides have an amidated C-terminus (Table S1).[1] The C-terminal amide increases these peptides' α-helical propensity[2] and promotes interactions with cellular membranes, which facilitates pore formation, thus conferring their membrane-lytic properties.[3] C-Terminal amidation is therefore crucial to study the native structure and dynamics of such peptides. This has been achieved by (1) harvesting the peptides from eukaryotic cells or organisms that do the post-translational modification;[4] (2) solid-phase peptide synthesis (SPPS) with a resin that results in a C-terminal amide after cleavage;[5] (3) recombinant expression in bacterial hosts followed by the enzymatic conversion of a C-terminal glycine into an amide;[6] or (4) recombinant expression of intein fusion proteins followed by cleavage in the presence of high concentrations of dithiothreitol and ammonium bicarbonate.[1,7]

Heteronuclear nuclear magnetic resonance (NMR) spectroscopy experiments require isotopic enrichment of ^{15}N, ^{13}C, and/or ^{2}H within the peptide. Site-specific labeling of ^{15}N and ^{13}C with SPPS quickly becomes cost-prohibitive with more than a handful of labeled residues. Moreover, many amino acids are not commercially available in triply labeled (^{2}H, ^{13}C, ^{15}N) form. Therefore, a fully ^{13}C,^{15}N-labeled, perdeuterated peptide must be expressed, rather than synthesized.

Previous NMR studies of uniformly labeled "melittin" neglected the C-terminal amide and simply studied recombinant melittin-COOH.[8,9] Due to the different equilibrium conditions of native melittin (melittin-$CONH_2$) and melittin-COOH, the α-helical structure was stabilized with additives such as trifluoroethanol,[9] which adversely impacts the peptide oligomerization.[10]

To produce triply labeled melittin, we chose to pursue a strategy consisting of recombinant expression of melittin-COOH in *E. coli* followed by chemical amidation to convert melittin-COOH into native melittin (Figure 1). Due to the toxicity of melittin in *E. coli*, melittin-COOH cannot be overexpressed by itself; it requires a fusion partner that inhibits its antimicrobial properties. A fusion protein consisting of a glutathione S-transferase (GST) solubility tag[11] followed by a flexible linker, tobacco etch virus (TEV) cleavage site, and melittin-COOH (Figure 1a) (hereafter referred to as GST-TEV-melittin-COOH) overexpresses after induction with 150 μM isopropyl β-D-1-thiogalactopyranoside at 18 °C (Figure S1). Inclusion of GST as the solubility tag facilitated the initial purification of GST-TEV-melittin-COOH with a GST affinity column. GST-TEV-melittin-COOH was then dialyzed into buffer suitable for TEV cleavage. Subsequent cleavage with TEV protease generates the native N-terminal glycine in melittin-COOH. The cleaved GST-TEV was separated from TEV protease and melittin-COOH with a GST affinity column prior to HPLC purification of melittin-COOH (Figure S2).

Prior to C-terminal amidation, the primary amines need to be protected so they cannot act as nucleophiles during the coupling reaction. Failure to protect these amines results in unwanted lactam formation during the subsequent coupling reaction. We note that since melittin has no acidic side chains, there was no need to protect carboxylic acid groups. However, in principle, a similar methodology could be used with peptides containing acidic residues if protection strategies are employed that selectively protect aspartic acid and glutamic acid side chains while retaining the C-terminal free carboxylic acid.[12]

For nucleophilic amine functional groups, we chose the Boc-protection strategy.[12] After an overnight reaction with di-*tert*-butyl dicarbonate (Boc_2O) and the organic base *N*,*N*-

Received: November 27, 2022
Published: February 8, 2023

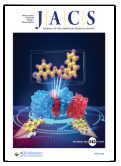

ACS Publications
Not subject to U.S. Copyright. Published 2023 by American Chemical Society

https://doi.org/10.1021/jacs.2c12631
J. Am. Chem. Soc. 2023, 145, 3850−3854

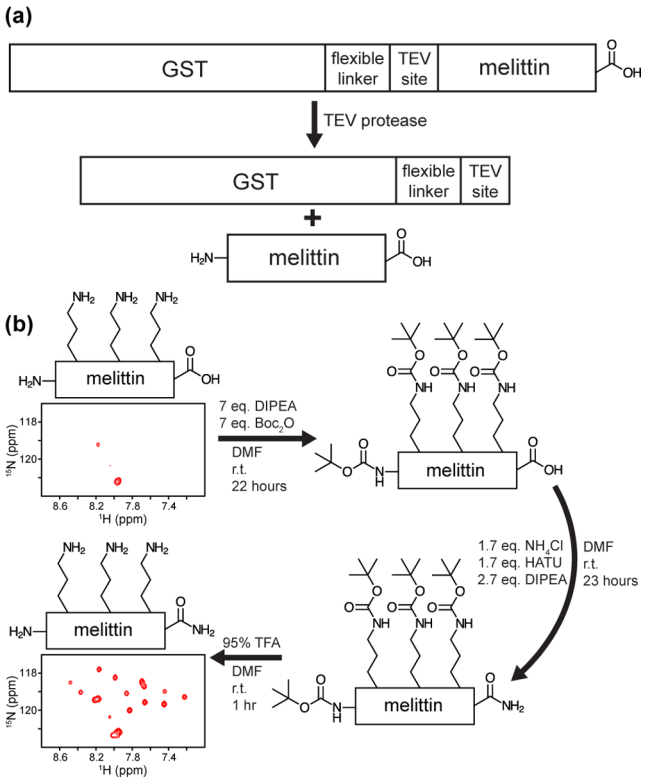

Figure 1. Schematic representation of (a) recombinant expression of melittin-COOH and (b) chemical amidation of melittin. Prior to chemical amidation, amines are Boc-protected. Following the amidation reaction, the Boc-protected groups are deprotected, leaving native melittin. $^{15}N-^{1}H$ HSQC spectra are shown for 1.0 mM ^{15}N-labeled melittin-COOH and native melittin-$CONH_2$. Each spectrum was collected on a 600 MHz spectrometer at 15 °C in 25 mM potassium phosphate pH 7.0, 50 mM NaCl, and 3% D_2O for 24 min. The melittin-COOH spectrum shows only a couple of peaks due to exchange broadening. Both spectra also show peaks corresponding to unfolded melittin outside of the spectral window depicted in this figure.

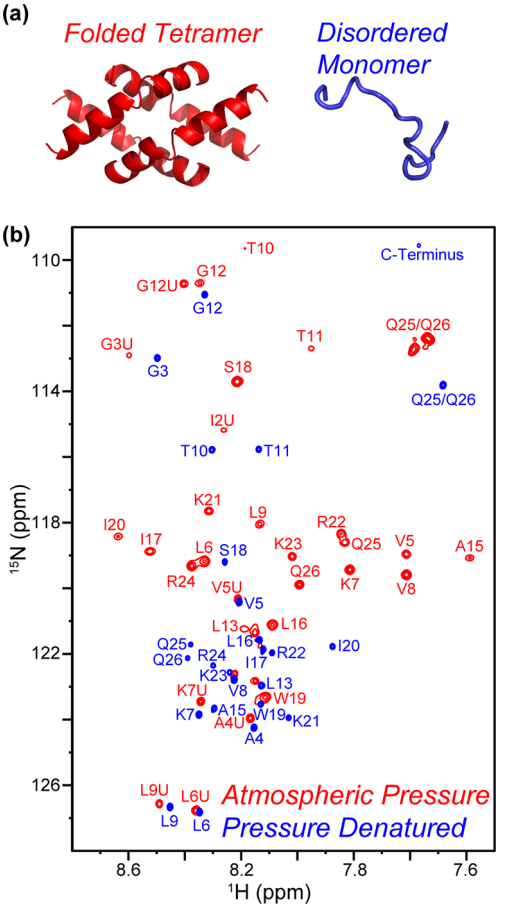

Figure 2. (a) Cartoon views of (left) α-helical, tetrameric, melittin and (right) disordered monomeric melittin. (b) $^{15}N-^{1}H$ HSQC spectra of melittin at atmospheric pressure (red) and pressure-denatured melittin at 2.25 kbar (blue). Peaks corresponding to the unfolded monomeric state at atmospheric pressure are denoted with a U after the residue name; resonances labeled in red without the U correspond to the folded, tetrameric state. Each spectrum was collected for 33 min on an 800 MHz spectrometer at 15 °C, with 1.0 mM $^{2}H,^{13}C,^{15}N$-labeled melittin in 25 mM phosphate buffer, pH 7.0, 50 mM NaCl, and 3% D_2O.

diisopropylethylamine (DIPEA) in *N,N*-dimethylformamide (DMF) followed by HPLC purification, we obtained Boc-protected melittin-COOH (Boc-melittin-COOH). Boc-melittin-COOH was then converted into an active ester with 1-[bis(dimethylamino)methylene]-1*H*-1,2,3-triazolo[4,5-*b*]-pyridinium 3-oxide hexafluorophosphate (HATU) in the presence of DIPEA in DMF. ^{15}N-Labeled NH_4Cl was then added to the solution to act as the nucleophile and attack the activated ester (Figure S3).[13] The use of $^{15}NH_4Cl$ makes incorporation of ^{15}N into the C-terminal amide inexpensive. After an overnight reaction, the solution was dried under a N_2 stream prior to deprotection in 95:5 trifluoroacetic acid (TFA):DMF and subsequent HPLC, ion exchange chromatography (Figure S4), and dialysis steps to obtain triply labeled native melittin.

With native melittin in hand, we sought to characterize its molecular structure in solution. Backbone chemical shift assignments were made using 3D TROSY-HNCA and 3D TROSY-HNCO spectra (Figure S5). The peptide was mostly tetrameric at atmospheric pressure, but pressure denatured with 2.25 kbar of hydrostatic pressure (Figure 2).[14] The use of pressure to denature the tetramer allows us to easily access both the folded and unfolded states without the need for chemical denaturants nor other changes in the buffer composition.[15] In the folded, tetrameric state, the N-terminal four residues' (G1−A4) signals are broadened below the detection limit. Residues assigned to the tetrameric state have secondary shifts indicative of α-helical secondary structure (Figure S5a,c,d).[16] Upon pressure denaturation, the chemical shifts are close to random coil values (Figure S5b), although an indication of transient α-helical character was observed through the small positive C^{α} secondary shifts for residues in the C-terminal half of the peptide.

Residual dipolar couplings (RDCs) are a sensitive probe of molecular structures in solution.[17] In the case of an α-helical peptide with an expected kink in it, like melittin, NMR-based orientation restraints can tightly define the relative orientation of the two α-helical segments.[18] We utilized the ARTSY[19] technique to measure backbone $^{1}D_{NH}$ RDCs in two separate alignment media, liquid crystalline Pf1 filamentous phage (Figure S6) and positively charged stretched polyacrylamide gel, on an 800 MHz spectrometer at 20 °C. Pf1 has a negatively charged surface that has strongly attractive, electrostatic interactions with positively charged melittin. To reduce these forces sufficiently and thereby obtain the degree

https://doi.org/10.1021/jacs.2c12631
J. Am. Chem. Soc. 2023, 145, 3850−3854

of melittin alignment needed to permit precise RDC measurements, high ionic strength buffer (25 mM phosphate pH 7.0, 700 mM NaCl) was used. Alignment in weakly positively charged gel is dominated by steric and repulsive electrostatic forces, and a low ionic strength buffer sufficed. If alignment forces were to impact the quaternary structure of melittin, contrast in the fits of the RDCs to the coordinates would show this, but RDCs measured in both media agreed comparably well with the structural models. Confirmed by the lack of chemical shift perturbation by the different media, we therefore conclude that the structure is not perturbed by the aligning media. We extracted alignment tensor parameters and predicted RDCs based on the structures using singular value decomposition (SVD) fitting of the experimental RDCs to the N−H bond vector orientations.[17] The principal axes of the alignment tensor must lie along the two C_2 symmetry axes of the melittin tetramer; therefore, only two fitted parameters (D_a and Rh) remain in the SVD fitting. The normalized scalar product between the two alignment tensors (~0.98) is high.[20] Thus, the tetramer alignments are very similar in gel and Pf1, despite the very different forces that determine the melittin alignment.

We generated 25 tetrameric models of melittin using the AlphaFold-Multimer[21] (AF-M) plugin to AlphaFold2[22] to compare to the experimental NMR data and the 2.0 Å X-ray crystal structure (PDB 2MLT) (Table S7).[23] To avoid bias toward pre-existing structures in the PDB that share large sequence identity with melittin, we excluded all structures with greater than 30% sequence identity to melittin from the training database. Due to AlphaFold2's inability to include post-translational modifications, we tested the effects of five different mutations on the quality of the structure prediction: melittin-COOH and melittin-COOH extended by a Lys, Arg, Gly, or Asp residue. Five AF-M models were generated for each mutant. The AF-M tetrameric models fell into two broad camps: structures with AF-M model confidence scores above 0.5 were in excellent agreement with the 2MLT crystal structure (backbone RMSD < 1.0 Å with respect to residues G1−K23), while the rest were inconsistent with the crystal structure (backbone RMSD > 4 Å) (Table S4; Figure S9c,d). We note that the angle of ~120° between the N- and C-terminal melittin helices, seen in both the crystal structure and the best AF-M models, differs significantly from the ~160° value seen by solid-state NMR for melittin traversing lipid bilayers.[24]

Remarkably, excluding the modified C-terminal helical turn (R24−Q26), our experimental $^1D_{NH}$ RDCs fit all of the AF-M models with confidence scores above 0.50 at least as well as, and often considerably better than, the 2MLT crystal structure (Figure 3; Figures S7, S8, S9a,b; Tables S4, S5). The top three AF-M models (Table S6), melittin-R-COOH #1, melittin-G-COOH #3, and melittin-K-COOH #1, had Q factors that were 20−48% better than the 2MLT crystal structure.

For comparison between the X-ray crystal structure and the AF-M models, the C-terminal Gln-26 $^1D_{NH}$ was excluded from the fit to the 2MLT crystal structure and all AF-M models due to evidence for dynamic disorder. Arg-24 and Gln-25 were also excluded from the SVD fits for AF-M models due to the non-native C-terminus disrupting the hydrogen-bonding pattern found in native melittin. We note that if Arg-24 and Gln-25 are excluded from the SVD fits for the 2MLT crystal structure, a Q factor of 0.21 is still obtained in Pf1 alignment media and 0.31 in stretched polyacrylamide gel, indicating that the different Q factors are indeed due to different qualities in the fits, rather than an artifact of using different sized data sets. Q factors below 0.20 are typically only seen for crystal structures with a resolution of 1.5 Å or better.[25] Therefore, our AF-M models provide a substantial improvement in structural resolution of the melittin tetramer compared to the 2.0 Å X-ray structure. Although AlphaFold2 does not yet support the inclusion of post-translational modifications, artificial mutations combined with experimental data can readily be used to validate the accuracy of such models.

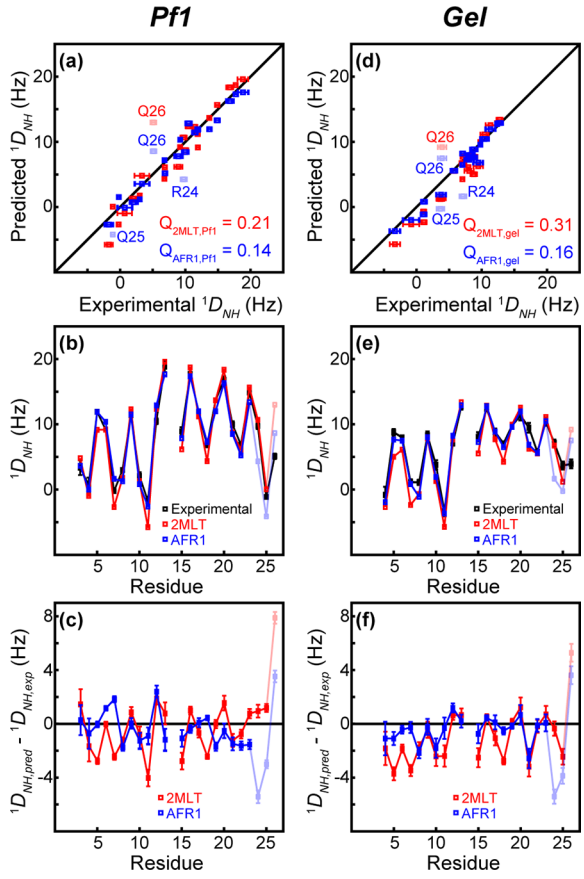

Figure 3. Agreement between the 2MLT crystal structure, best fitting AlphaFold-Multimer model, and experimental RDCs. (a−c) RDCs measured in Pf1. (d−f) RDCs measured in stretched polyacrylamide gel. (a, d) Averaged predicted vs experimental RDC correlation plot for the 2MLT crystal structure (red) and the best scoring AF-M model with a C-terminal arginine extension (AFR1) (blue). Q = RMS($\langle D_{exp}\rangle - D_{pred}$)/sqrt($D_a^2[4 + 3Rh^2]/5$), where D_a (Hz) is the magnitude of the dipolar coupling tensor and Rh is the rhombicity. (b, e) Residue-specific experimental and averaged predicted $^1D_{NH}$ RDCs. (c, f) Residuals between the averaged predicted and experimental RDCs. C-Terminal RDCs that were excluded from the SVD fit are semitransparent.

Our work presents the first example of the production of uniformly triply labeled melittin with its native amidated C-terminus. Previous NMR studies relied on naturally occurring melittin without isotopic enrichment,[4] synthetic melittin with site specific labeling,[5] or recombinant melittin-COOH.[9] Since its introduction, AlphaFold2 has demonstrated its ability to accurately predict numerous protein structures[26] as validated by RDC measurements.[27,28] Our results show that also for oligomers AF-M generates models that agree better with solution RDCs than a good-quality X-ray crystal structure. AlphaFold2 and AF-M structure predictions, followed by

https://doi.org/10.1021/jacs.2c12631
J. Am. Chem. Soc. 2023, 145, 3850−3854

confirmation of the correct structure with RDCs, will prove useful for future structural biology studies either where there is no crystal structure available or for instances in which the crystal structure was solved to lower resolution than needed to fully take advantage of the wealth of information afforded by precise measurements like RDCs.

The production of isotopically labeled native melittin has facilitated the application of solution state NMR to study the molecular structure of melittin in solution at high precision and opens the door for the use of advanced NMR techniques to study melittin's folding/oligomerization processes[29,30] along with its membrane-lytic biological function.[31] We foresee this strategy consisting of recombinant expression followed by chemical post-translational modification to be broadly applicable for studies where the post-translational modification is crucial for the native structure or function.

■ ASSOCIATED CONTENT

Supporting Information

The Supporting Information is available free of charge at https://pubs.acs.org/doi/10.1021/jacs.2c12631.

Detailed description of the production of isotopically labeled native melittin; NMR sample preparation and NMR spectroscopy; data processing, structural model development, and analysis; purification characterization and chromatograms; supplementary spectra; and tables with amidated antimicrobial peptides, melittin chemical shifts, melittin RDCs, and RDC fits to structural models (PDF)

Accession Codes

The BMRB accession code for tetrameric melittin chemical shifts, monomeric chemical shifts, and tetrameric melittin RDCs is 51703.

■ AUTHOR INFORMATION

Corresponding Author

Ad Bax − *Laboratory of Chemical Physics, NIDDK, National Institutes of Health, Bethesda, Maryland 20892-0520, United States;* orcid.org/0000-0002-9809-5700; Email: bax@nih.gov

Author

Martin D. Gelenter − *Laboratory of Chemical Physics, NIDDK, National Institutes of Health, Bethesda, Maryland 20892-0520, United States;* orcid.org/0000-0002-6412-805X

Complete contact information is available at: https://pubs.acs.org/10.1021/jacs.2c12631

Notes

The authors declare no competing financial interest.

■ ACKNOWLEDGMENTS

We thank Y. Shen, J. Ying, J. L. Baber, and J. Lloyd for technical support; T. Schmidt, J. M. Louis, S. C. Chiliveri, E. Masoumzadeh, T. Kakeshpour, D. A. Torchia, W. M. Yau, R. Tycko, and J. Jumper for insightful discussions; A. M. Calvey for stretched polyacrylamide gel sample preparation; and G. Abdoulaeva for peptide synthesis. This work was supported by the Intramural Research Program of the National Institute of Diabetes and Digestive and Kidney Diseases (DK075141).

■ REFERENCES

(1) Zhu, S.; Weber, D. K.; Separovic, F.; Sani, M.-A. Expression and Purification of the Native C-Amidated Antimicrobial Peptide Maculatin 1.1. *J. Pept. Sci.* **2021**, *27* (8), No. e3330.

(2) Dennison, S. R.; Phoenix, D. A. Influence of C-Terminal Amidation on the Efficacy of Modelin-5. *Biochemistry* **2011**, *50* (9), 1514−1523.

(3) Strandberg, E.; Tiltak, D.; Ieronimo, M.; Kanithasen, N.; Wadhwani, P.; Ulrich, A. S. Influence of C-Terminal Amidation on the Antimicrobial and Hemolytic Activities of Cationic α-Helical Peptides. *Pure Appl. Chem.* **2007**, *79* (4), 717−728.

(4) Brown, L. R.; Lauterwein, J.; Wüthrich, K. High-Resolution 1H-NMR Studies of Self-Aggregation of Melittin in Aqueous Solution. *Biochim. Biophys. Acta BBA - Protein Struct.* **1980**, *622* (2), 231−244.

(5) Wilson, C. B.; Tycko, R. Millisecond Time-Resolved Solid-State NMR Initiated by Rapid Inverse Temperature Jumps. *J. Am. Chem. Soc.* **2022**, *144* (22), 9920−9925.

(6) Wu, B.; Wijma, H. J.; Song, L.; Rozeboom, H. J.; Poloni, C.; Tian, Y.; Arif, M. I.; Nuijens, T.; Quaedflieg, P. J. L. M.; Szymanski, W.; Feringa, B. L.; Janssen, D. B. Versatile Peptide C-Terminal Functionalization via a Computationally Engineered Peptide Amidase. *ACS Catal.* **2016**, *6* (8), 5405−5414.

(7) Rodriguez Camargo, D. C.; Tripsianes, K.; Kapp, T. G.; Mendes, J.; Schubert, J.; Cordes, B.; Reif, B. Cloning, Expression and Purification of the Human Islet Amyloid Polypeptide (HIAPP) from Escherichia Coli. *Protein Expr. Purif.* **2015**, *106*, 49−56.

(8) Ishida, H.; Nguyen, L. T.; Gopal, R.; Aizawa, T.; Vogel, H. J. Overexpression of Antimicrobial, Anticancer, and Transmembrane Peptides in Escherichia Coli through a Calmodulin-Peptide Fusion System. *J. Am. Chem. Soc.* **2016**, *138* (35), 11318−11326.

(9) Ramirez, L.; Shekhtman, A.; Pande, J. Nuclear Magnetic Resonance-Based Structural Characterization and Backbone Dynamics of Recombinant Bee Venom Melittin. *Biochemistry* **2018**, *57* (19), 2775−2785.

(10) Othon, C. M.; Kwon, O.-H.; Lin, M.; Zewail, A. H. Solvation in Protein (Un)Folding of Melittin Tetramer-Monomer Transition. *Proc. Natl. Acad. Sci. U.S.A.* **2009**, *106* (31), 12593−12598.

(11) Zhou, L.; Liu, Z.; Xu, G.; Li, L.; Xuan, K.; Xu, Y.; Zhang, R. Expression of Melittin in Fusion with GST in *Escherichia Coli* and Its Purification as a Pure Peptide with Good Bacteriostatic Efficacy. *ACS Omega* **2020**, *5* (16), 9251−9258.

(12) Isidro-Llobet, A.; Álvarez, M.; Albericio, F. Amino Acid-Protecting Groups. *Chem. Rev.* **2009**, *109* (6), 2455−2504.

(13) Zou, X.; Liu, C.; Li, C.; Fu, R.; Xu, W.; Bian, H.; Dong, X.; Zhao, X.; Xu, Z.; Zhang, J.; Shen, Z. Study on the Structure-Activity Relationship of Dihydroartemisinin Derivatives: Discovery, Synthesis, and Biological Evaluation of Dihydroartemisinin-Bile Acid Conjugates as Potential Anticancer Agents. *Eur. J. Med. Chem.* **2021**, *225*, 113754.

(14) Thompson, R. B.; Lakowicz, J. R. Effect of Pressure on the Self-Association of Melittin. *Biochemistry* **1984**, *23* (15), 3411−3417.

(15) Caro, J. A.; Wand, A. J. Practical Aspects of High-Pressure NMR Spectroscopy and Its Applications in Protein Biophysics and Structural Biology. *Methods* **2018**, *148*, 67−80.

(16) Kjaergaard, M.; Poulsen, F. M. Sequence Correction of Random Coil Chemical Shifts: Correlation between Neighbor Correction Factors and Changes in the Ramachandran Distribution. *J. Biomol. NMR* **2011**, *50* (2), 157−165.

(17) Losonczi, J. A.; Andrec, M.; Fischer, M. W. F.; Prestegard, J. H. Order Matrix Analysis of Residual Dipolar Couplings Using Singular Value Decomposition. *J. Magn. Reson.* **1999**, *138* (2), 334−342.

(18) Wright, A. K.; Paulino, J.; Cross, T. A. Emulating Membrane Protein Environments−How Much Lipid Is Required for a Native Structure: Influenza S31N M2. *J. Am. Chem. Soc.* **2022**, *144* (5), 2137−2148.

(19) Fitzkee, N. C.; Bax, A. Facile Measurement of 1H-15N Residual Dipolar Couplings in Larger Perdeuterated Proteins. *J. Biomol. NMR* **2010**, *48* (2), 65−70.

(20) Prestegard, J. H.; Al-Hashimi, H. M.; Tolman, J. R. NMR Structures of Biomolecules Using Field Oriented Media and Residual Dipolar Couplings. *Q. Rev. Biophys.* **2000**, *33* (4), 371−424.
(21) Evans, R.; O'Neill, M.; Pritzel, A.; Antropova, N.; Senior, A.; Green, T.; Žídek, A.; Bates, R.; Blackwell, S.; Yim, J.; Ronneberger, O.; Bodenstein, S.; Zielinski, M.; Bridgland, A.; Potapenko, A.; Cowie, A.; Tunyasuvunakool, K.; Jain, R.; Clancy, E.; Kohli, P.; Jumper, J.; Hassabis, D. Protein Complex Prediction with AlphaFold-Multimer. *bioRxiv*. March 10, 2022. DOI: 10.1101/2021.10.04.463034 (accessed 2022−11−18).
(22) Jumper, J.; Evans, R.; Pritzel, A.; Green, T.; Figurnov, M.; Ronneberger, O.; Tunyasuvunakool, K.; Bates, R.; Žídek, A.; Potapenko, A.; Bridgland, A.; Meyer, C.; Kohl, S. A. A.; Ballard, A. J.; Cowie, A.; Romera-Paredes, B.; Nikolov, S.; Jain, R.; Adler, J.; Back, T.; Petersen, S.; Reiman, D.; Clancy, E.; Zielinski, M.; Steinegger, M.; Pacholska, M.; Berghammer, T.; Bodenstein, S.; Silver, D.; Vinyals, O.; Senior, A. W.; Kavukcuoglu, K.; Kohli, P.; Hassabis, D. Highly Accurate Protein Structure Prediction with AlphaFold. *Nature* **2021**, *596* (7873), 583−589.
(23) Terwilliger, T. C.; Eisenberg, D. The Structure of Melittin. I. Structure Determination and Partial Refinement. *J. Biol. Chem.* **1982**, *257* (11), 6010−6015.
(24) Smith, R.; Separovic, F.; Milne, T. J.; Whittaker, A.; Bennet, F. M.; Cornell, B. A.; Makriyannis, A. Structure and Orientation of the Pore-Forming Peptide, Melittin, in lipid Bilayers. *J. Mol. Biol.* **1994**, *241*, 456−466.
(25) Chen, K.; Tjandra, N. The Use of Residual Dipolar Coupling in Studying Proteins by NMR. *Top. Curr. Chem.* **2011**, *326*, 47−67.
(26) Jones, D. T.; Thornton, J. M. The Impact of AlphaFold2 One Year On. *Nat. Methods* **2022**, *19* (1), 15−20.
(27) Zweckstetter, M. NMR Hawk-Eyed View of AlphaFold2 Structures. *Protein Sci.* **2021**, *30* (11), 2333−2337.
(28) Robertson, A. J.; Courtney, J. M.; Shen, Y.; Ying, J.; Bax, A. Concordance of X-Ray and AlphaFold2Models of SARS-CoV-2 Main Protease with Residual Dipolar Couplings Measured in Solution. *J. Am. Chem. Soc.* **2021**, *143* (46), 19306−19310.
(29) Rennella, E.; Sekhar, A.; Kay, L. E. Self-Assembly of Human Profilin-1 Detected by Carr−Purcell−Meiboom−Gill Nuclear Magnetic Resonance (CPMG NMR) Spectroscopy. *Biochemistry* **2017**, *56* (5), 692−703.
(30) Barnes, C. A.; Robertson, A. J.; Louis, J. M.; Anfinrud, P.; Bax, A. Observation of β-Amyloid Peptide Oligomerization by Pressure-Jump NMR Spectroscopy. *J. Am. Chem. Soc.* **2019**, *141* (35), 13762−13766.
(31) van den Bogaart, G.; Guzmán, J. V.; Mika, J. T.; Poolman, B. On the Mechanism of Pore Formation by Melittin. *J. Biol. Chem.* **2008**, *283* (49), 33854−33857.

https://doi.org/10.1021/jacs.2c12631
J. Am. Chem. Soc. 2023, 145, 3850−3854